Tuning Side Chain and Main Chain Order in a Prototypical Donor–Acceptor Copolymer: Implications for Optical, Electronic, and Photovoltaic Characteristics

Marcel Schubert, Johannes Frisch, Sybille Allard, Eduard Preis, Ullrich Scherf, Norbert Koch, and Dieter Neher

Contents

M. Schubert (✉)
Soft Matter Photonics, School of Physics and Astronomy, University of St Andrews, KY16 9SS St Andrews, UK
e-mail: ms293@st-andrews.ac.uk

J. Frisch
Institut für Physik and IRIS Adlershof, Humboldt-Universität zu Berlin, Brook-Taylor-Straße 6, 12489 Berlin, Germany
e-mail: johannes.frisch@helmholtz-berlin.de

S. Allard • E. Preis • U. Scherf
Macromolecular Chemistry and Institute for Polymer Technology, Bergische Universität Wuppertal, Gaußstraße 20, 42119 Wuppertal, Germany
e-mail: sallard@uni-wuppertal.de; preis@uni-wuppertal.de; scherf@uni-wuppertal.de

N. Koch
Institut für Physik and IRIS Adlershof, Humboldt-Universität zu Berlin, Brook-Taylor-Straße 6, 12489 Berlin, Germany

Helmholtz Zentrum Berlin für Materialien und Energie GmbH, Albert-Einstein-Straße 15, 12489 Berlin, Germany
e-mail: norbert.koch@physik.hu-berlin.de

D. Neher
Physics of Soft Matter, School of Physics and Astronomy, University of Potsdam, 14476 Potsdam, Germany
e-mail: neher@uni-potsdam.de

K. Leo (ed.), *Elementary Processes in Organic Photovoltaics*,
Advances in Polymer Science 272, DOI 10.1007/978-3-319-28338-8_10

Abstract The recent development of donor–acceptor copolymers has led to an enormous improvement in the performance of organic solar cells and organic field-effect transistors. Here we describe the synthesis, detailed characterisation, and application of a series of structurally modified copolymers to investigate fundamental structure–property relationships in this class of conjugated polymers. The interplay between chemical structure and optoelectronic properties is investigated. These are further correlated to the charge transport and solar cell performance, which allows us to link their chemical structure to the observed physical properties.

Keywords Aggregate states • All-polymer heterojunctions • Alternating copolymers • Ambipolar charge transport • Ambipolar materials • Backbone modifications • Bilayer solar cells • Charge separation • Conformational disorder • Crystalline phases • Donor–acceptor copolymers • Electron traps • Energetic disorder • Energy-level alignment • Fermi-level alignment • Fermi-level pinning • Interface dipole • Interlayer • Intrachain order • Intragap states • Microscopic morphology • Mobility imbalance • Mobility relaxation • Monte Carlo simulation • Multiple trapping model • Nonradiative recombination • OFET • Open-circuit voltage • Optoelectronic properties • Partially alternating copolymers • Photo-CELIV • Photocurrent • Photovoltaic gap • Polymer intermixing • Recombination losses • Spectral diffusion • Statistical copolymers • Stille-type cross-coupling • Structure–property relationships • Time-dependent mobility • Time-of-flight (TOF) • Transient photocurrent • Ultraviolet photoelectron spectroscopy • Vacuum-level alignment • X-ray photoelectron spectroscopy

1 Introduction to Donor–Acceptor Copolymers

The development and optimization of donor–acceptor (D–A) copolymers has greatly improved the performance of conjugated polymers over the past decade. Comprising an electron-rich (donor) and an electron-deficient (acceptor) molecular building block, these copolymers allow the systematic and easy modification of the material's optoelectronic properties [1] (Fig. 1). They can be widely tuned with respect to their optical bandgap and molecular frontier orbitals. Most impressively, the charge carrier mobility of the latest generation of D–A copolymers exceeds values of 10 cm^2/Vs [2, 3]. Being on a par with the performance of amorphous silicon and other inorganic semiconductors renders them the ideal materials for applications such as organic thin-film transistors, inverters, and circuitry. Furthermore, they dis-

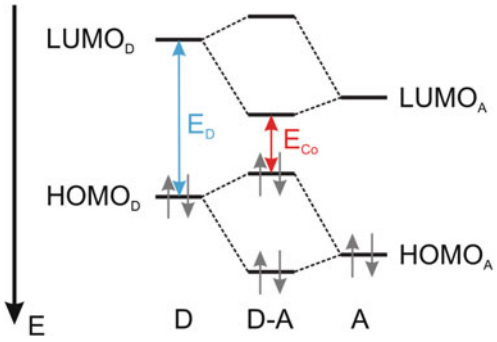

Fig. 1 Energy scheme illustrating the working principle of copolymers built up by the covalent binding of an electron-deficient acceptor (A) unit with an electron-rich donor (D) fragment. Due to the hybridization of the frontier molecular orbitals, the bandgap of the copolymer (E_{Co}) is strongly reduced compared to those of the donor (E_D) or acceptor block. For a rough estimate, E_{Co} is given by the energy difference between the highest occupied molecular orbital of the donor and the lowest unoccupied molecular orbital of the acceptor, while there are more chemical and physical parameters that can affect the bandgap [1]

play a class of organic semiconductors that comprises a large number of ambipolar materials, which possess comparable mobilities for electrons and holes [4].

The concept of combining chemically and structurally different monomer units into one backbone promoted the development of an enormous number of copolymer structures with an equal variety of physical and chemical properties. Consequently, D–A copolymers are now the first choice for the donor component in organic solar cells, where being able to precisely adjust the energetic and optical properties is of fundamental importance. On the other hand, they can also be incorporated as electron acceptors because of their high electron mobilities [5–8]. So-called all-polymer solar cells, which combine both donor and acceptor polymers, have recently demonstrated efficiencies above 5 % [9–11]. Thus, electron-transporting D–A copolymers have the potential to rival the dominating role of fullerene-based acceptors, which have been the predominant acceptors in organic solar cells for more than 20 years. Even copolymers with very similar chemical structures can now be combined as donor and acceptor within the same active layer [12], potentially avoiding difficulties arising from the different mechanical properties of polymers and small molecules.

In addition to tuning the electronic properties, D–A copolymers offer a wide variability in the nature and sequence of the side chains, thereby controlling packing and interchain interaction and opening exciting opportunities for the control of the blend morphology [13].

Another approach that is not yet in widespread use is breaking the strict alternation of the donor and acceptor units along the copolymer backbone, thereby altering the intrachain order. It is expected that the transition from strictly alternating to partially alternating or even statistical copolymer will result in subtle changes to the optical, electronic, and charge transport properties, with important consequences

for their application in photovoltaic devices. Theoretical work and numerical simulations have indeed proposed that imbalanced electron and hole mobilities as well as an increased degree of energetic disorder of the donor and acceptor material may assist the split of electron–hole pairs at D–A heterojunctions [14–16]. Manipulating the energetic disorder by changing the intrachain order is an attractive approach to experimentally investigate this correlation.

Here we summarize the synthesis and investigation of a series of D–A copolymers with 9,9-dialkylfluorene (F) and 4,7-di(thiophene-2-yl)-2,1,3-benzothiadiazole (TBTT) building blocks in different arrangements. Poly(FTBTT) (PFTBTT) copolymers are prototypical, given that they were among the first D–A-type copolymers designed especially for use in organic solar cells [17]. Since then various studies have investigated the charge generation and charge recombination processes, ultrafast photophysics, and morphology of PFTBTT-based solar cells [18–26].

2 Synthesis of Alternating and Partially Alternating PFTBTT Copolymers

The aim of the synthetic part was generating a series of structurally modified D–A copolymers. Additional goals were having a sufficiently high electron mobility to apply them as the acceptor component in all-polymer solar cells and investigating the influence of the degree of intrachain order on the charge carrier mobility and photovoltaic performance.

First, two alternating copolymers were investigated, alt-PF8TBTT with linear octyl and alt-PF8/12TBTT with branched octyldodecyl substituents attached to the fluorene unit. The change from linear to branched side chains was expected to alter the interchain order in the solid state, thus also affecting the charge carrier mobility and device performance.

The copolymers were synthesized from 2,7-dibromo-9,9-dialkyl fluorene [27] and distannylated TBTT in a Stille-type cross-coupling reaction following procedures described in the literature [28, 29] (Fig. 2). Copolymer alt-PF8TBTT was isolated with a molecular weight M_n of 5000 g/mol and a polydispersity index (PDI) of 2.0–2.5. Copolymer alt-PF8/12TBTT was generated with a molecular weight M_n of 8000 g/mol and a PDI of 2.1.

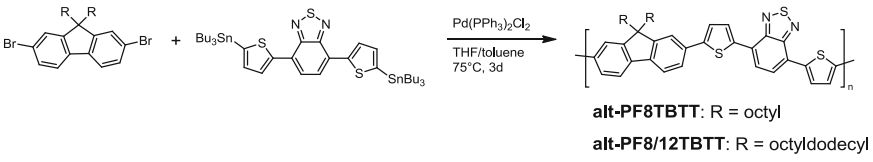

Fig. 2 Synthesis of alternating PFTBTT copolymers via Stille-type coupling reactions

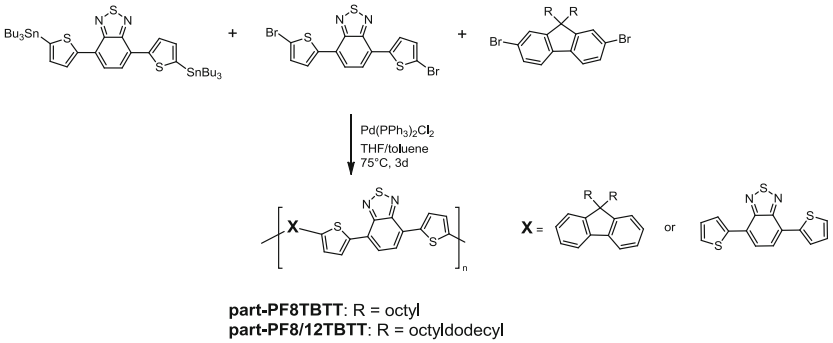

Fig. 3 Synthesis of partially alternating copolymers via a Stille-type coupling reaction that introduces a higher TBTT content into the backbone. The enrichment is estimated to be about 5 % compared to the alternating copolymer, yielding blocks of several directly connected TBTT units

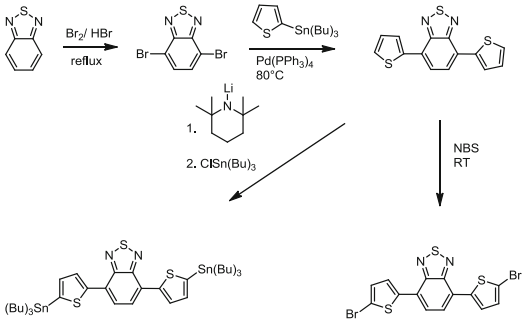

Fig. 4 Monomer synthesis of the distannylated TBTT (*left*) and the dibrominated TBTT (*right*)

To increase the intrachain disorder, we also synthesized two partially alternating copolymers, part-PF8TBTT and part-PF8/12TBTT, in a Stille-type cross-coupling reaction starting with 2,7-dibromo-9,9-dialkyl fluorene, distannylated TBTT, and dibromo TBTT, in which the TBTT monomer unit was randomly connected to TBTT or fluorene units (Fig. 3).

The monomer syntheses followed literature procedures, while the concept of partially alternating copolymers displayed a novel attempt to gradually degrade the otherwise perfect alternation of D–A copolymers [28–33]. The monomer syntheses of dibromo or distannylated TBTT starting from benzothiadiazole are illustrated in Fig. 4. The stoichiometry was adjusted to equimolar amounts of bromo and stannyl functions. Further analysis revealed that these partially alternating copolymers contain a TBTT content of about 50 %. Thus, the overall composition is comparable to those of the alternating copolymers. However, according to Fig. 3, the partially alternating copolymers contain blocks of several directly connected TBTT units although the probability for the formation of these blocks is rather small. Table 1 summarizes the molecular weights and optical properties of all copolymers.

Table 1 Number- (M_n) and weight-averaged (M_w) molecular masses, polydispersity (PDI), and maximum absorbance (Abs_{max}) in chloroform of all copolymers used in this study. Copolymer structures: *alt,* alternating; *part,* partially alternating; *stat,* statistical. Side chains: 8 = octyl; 8/12 = octyldodecyl; 2/6 = ethylhexyl; 3/12 = farnesyl

	M_n (g/mol)	M_w (g/mol)	PDI (M_w/M_n)	Abs_{max} ($CHCl_3$) (nm)
alt-PF8TBTT	5000	10,000	2.00	384, 536
alt-PF8/12TBTT	8000	17,000	2.12	384, 536
alt-PF3/12TBTT	4900	13,300	2.71	357, 530
part-PF8TBTT	3000	5000	1.66	378, 536
part-PF8/12TBTT	8200	13,000	1.58	378, 542
stat-PF2/6TBTT (30 % TBTT)	10,000	20,000	2	355, 522
stat-PF3/12TBTT (2 % TBTT)	10,000	15,000	1.5	–

To alter the copolymer structure even stronger, we synthesized statistical PFTBTTs according to Yamamoto-type homo-coupling of the two dibrominated monomers [33, 34]. The resulting copolymers showed a higher molecular weight but only a maximum TBTT content of about 30 % by using a monomer molar ratio of 60:40 (TBTT:F) (see Table 1). A series of Yamamoto-type reactions showed that the incorporation ratio of TBTT depends less on the monomer ratio used, revealing a lower reactivity of the electron-poor building block into the polymer chains. Because of their gradually increasing TBTT content (from about 2–30 %), statistical copolymers were used to investigate the effect of the polymer backbone composition on the copolymers' optoelectronic properties.

3 Energetic and Optical Properties of Pristine Copolymers

In order to characterize the alteration of the physical properties introduced by the chemical modifications, we first present a thorough investigation of the energetic structure and optical properties of a series of different PFTBTT copolymers. Structurally different backbone modifications are introduced with so-called partially alternating copolymers. Finally, we compare alternating and partially alternating copolymers with different side chains.

3.1 Influence of Acceptor Concentration in D–A Copolymers on the Energy-Level Alignment

To determine the effects of different acceptor concentrations on the optical and electronic properties, we investigated spin-coated films of different PFTBTT copolymers on poly(3,4-ethylene dioxy thiophene):poly(styrene sulfonic acid) (PEDT:PSS) substrates. The PEDT:PSS was used to ensure the same polymer

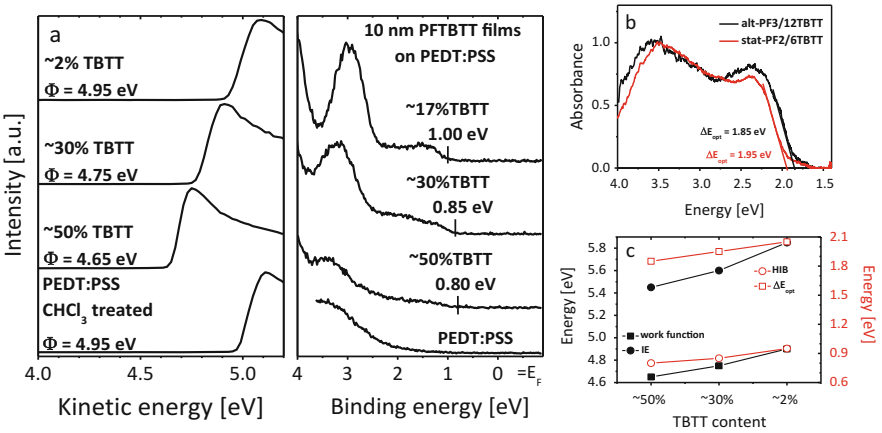

Fig. 5 (**a**) Secondary electron cutoff (*left*) and valence band spectra (*right*) of spin-coated 10-nm PFTBTT films on PEDT:PSS substrates. Polymer films differ in the acceptor (TBTT) content value, from ∼50 % for alternating copolymers to ∼30 and 2 % for statistical copolymers. (**b**) Ultraviolet–visible spectroscopy (UV-Vis) absorption spectra of spin-coated 10-nm alt-PF3/12TBTT (*black*) and stat-PF2/6TBTT (*red*) films on PEDT:PSS substrates. The absorption spectra of PEDT:PSS were subtracted. (**c**) Work function, ionization energy, hole injection barrier, and ΔE_{opt} (optical gap) of PFTBTT films with varying TBTT content on top of PEDT:PSS substrates determined by ultraviolet photoelectron spectroscopy and UV-Vis measurements

layer morphology as in the electrical and optoelectronic studies. The acceptor concentration was varied among ∼50 % (alt-PF3/12TBTT), ∼30 % (stat-PF2/6TBTT), and ∼2 % (stat-PF3/12TBTT), and the energy-level alignment was probed with ultraviolet photoelectron spectroscopy (UPS). From these measurements, we determined the secondary electron cutoff (SECO) and valence band (VB) spectra, which reveal the work function (Φ) and valence band onset of the copolymers on top of PDOT:PSS, respectively.

SECO and VB spectra of the different copolymers and of the PEDT:PSS electrode are shown in Fig. 5a. As the acceptor (TBTT) content increases, the emission feature at 2.7 eV shifts to higher binding energy and broadens, whereas the VB onset elongates toward the Fermi energy (E_F). However, Φ and the hole injection barrier (HIB) decrease with increasing acceptor content. Consequently, the ionization energy (IE) changes from 5.45 eV (∼50 % TBTT) to 5.60 eV (∼30 % TBTT) and to 5.85 eV (∼2 % TBTT). The value for low TBTT content is close to that found in pure polyfluorene, where the IE was determined to be 5.75 eV [35]. Note that the substrate work function did not change after deposition of a PFTBTT film with ∼2 % acceptor content, suggesting an established vacuum-level alignment. This situation changes for higher acceptor concentrations and, thus, smaller IEs. The substrate Φ decreases almost linearly with increasing acceptor content to 4.75 eV (∼30 % TBTT) and 4.65 eV (∼50 % TBTT). Accordingly, the Φ value where the transition between vacuum-level alignment and Fermi-level pinning occurs is far below 4.95 eV for higher acceptor content in PFTBTT copolymers. Consequently,

pinning of the Fermi level occurs at intragap states between the VB maximum and E_F, whose density is expected to be well below the sensitivity of the present UPS experimental setup [36–38]. Such high densities of gap states could potentially hinder the charge transport within the PFTBTT phase and could also negatively affect the photovoltaic performance.

Similar results can be found for the optical gap (ΔE_{opt}) determined by the onset of the optical absorption spectra (see Fig. 5b). The onset is shifted by 0.1 eV to higher energies upon decreasing the acceptor content from ~50 to ~30 %. The optical gap is further increased to 2.05 eV for lower acceptor concentrations (see Fig. 5c). By subtracting ΔE_{opt} from the IE, we can estimate the electron affinity (EA) of the polymers. Accordingly, the acceptor concentration changes both the IE and the EA. The characteristic values (Φ, HIB, ΔE_{opt} and IE) are summarized in Fig. 5c as a function of the acceptor concentration. Note that the HIB does not change in parallel to the IE. Therefore, calculating the VB onset position with respect to the Fermi level, assuming vacuum-level alignment at the polymer/PEDT:PSS interface, fails for PFTBTT films with ~30 and ~50 % acceptor concentrations because of the pinning of the Fermi level at intragap states.

3.2 *Aggregation Effects in Partially Alternating Copolymers*

Partially alternating copolymers were synthesized in order to have a lower degree of structural disorder compared to the statistical copolymers discussed above. Although the chemical modifications we introduced are only minor, the direct comparison between partially alternating copolymers and their alternating counterparts reveals distinct changes to the optical properties. Absorption spectra for copolymers with two different side chain substitutions in solution and in thin spin-coated films are displayed in Fig. 6. In solution, partially alternating copolymers show broadened absorption spectra, again indicating an increase in the energetic disorder. In addition,

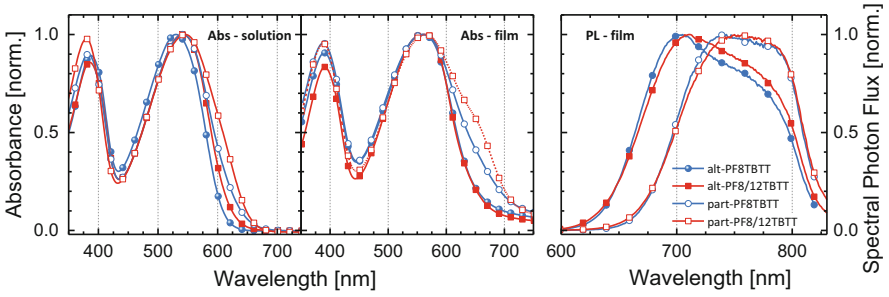

Fig. 6 Normalized absorbance (Abs) of alternating (*closed symbols*) and partially alternating (*open symbols*) PFTBTT copolymers measured in solution (*left*) and in thin film (*middle*). Also shown are normalized photoluminescence film spectra (*right*)

the thin-film absorption of the partially alternating copolymers is redshifted by about 0.15–0.2 eV. This shift is caused by the appearance of an additional absorption shoulder centered at about 650 nm, while the two main absorption bands around 375 and 550 nm remain clearly visible in all four derivatives. A redshift is also observed in the photoluminescence spectra, which proves that the partially alternating copolymers comprise a reduced optical bandgap. The appearance of such spectral features has been assigned to aggregate states that form upon the aggregation or crystallization of conjugated polymers; they are redshifted because of an improved planarization of the backbone [39, 40]. Furthermore, these states dominate the emission characteristics because of their fast spectral diffusion into these lower-energy states. The formation of aggregate states is further supported by the absorption spectra recorded in a good solvent (chloroform) and at low concentration (0.1 g/L), where the formation of aggregates is suppressed [20, 40, 41]. Most likely, aggregation of the partially alternating moieties is induced by multiple connected TBTT segments that induce stacking of neighbored chains. On the other hand, we attribute the absence of the red-edge absorbance in alternating and statistical copolymers to a rather disordered and amorphous film morphology, which is consistent with the reported absence of X-ray diffraction signals in alt-PF8TBTT [20].

4 Charge Transport Properties of Alternating, Partially Alternating, and Statistical Copolymers

Ambipolar charge transport for the PFTBTT-type copolymer F8TBT was first demonstrated in a light-emitting organic field-effect transistor (OFET) structure [21]. Figure 7 displays OFET characteristics measured in a bottom gate–top electrode geometry with a silanized silicon dioxide gate insulator. The latter was introduced to prevent electron trapping at the interface between the gate dielectric and the conjugated polymer [42]. Ambipolar charge transport in alt-PF8TBTT is clearly visible with mobilities for holes and electrons of $\mu_h = 2 \times 10^{-3}$ cm^2/Vs and $\mu_e = 4 \times 10^{-4}$ cm^2/Vs, respectively. Thus, alt-PF8TBTT and related copolymers can be regarded as ambipolar materials with an almost balanced electron and hole transport. This is consistent with the excellent acceptor properties of alt-PF8/12TBTT in organic solar cells [25].

Transient photocurrent measurements were performed to address the bulk electron transport in the three different copolymer structures. The technique of photogenerated charge extraction by linearly increasing voltage (photo-CELIV) is applied because it allows us to probe time-dependent charge transport phenomena in organic layers with active layer thicknesses of about 100 nm [43]. A charge-generation layer was introduced in the devices to ensure that the transport of electrons is measured [44]. Extracted electron mobilities are displayed in Fig. 8. The mobility differs by almost two orders of magnitude and is clearly related to the degree of structural

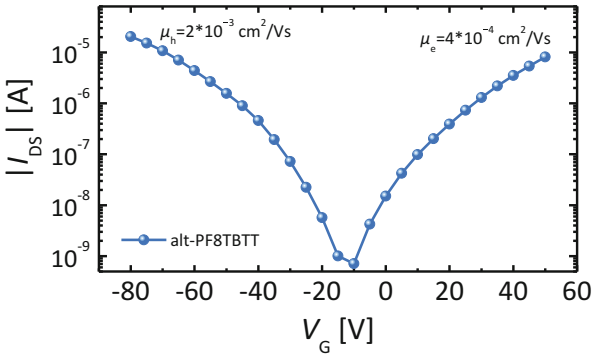

Fig. 7 Transfer characteristic of alt-PF8TBTT in bottom gate field-effect transistor at a source-drain voltage of −80 V

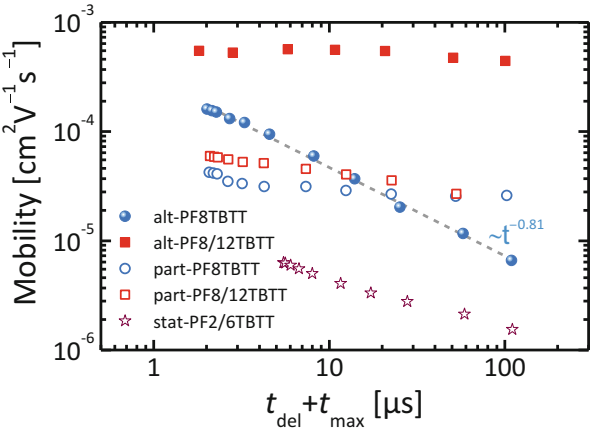

Fig. 8 Photogenerated charge extraction by linearly increasing voltage (photo-CELIV) results for the electron mobility of alternating (*filled squares* and *spheres*), partially alternating (*open squares* and *circles*), and statistical (*open stars*, 32 % TBTT) PFTBTT copolymers. To improve charge generation, all devices featured a 3-nm-thin P3HT charge-generation layer. Complete device structure: ITO/PEDT:PSS/P3HT-IL/PFTBTT/Sm/Al; device area: 1 mm^2. Layer thickness: P3HT-IL = 3 nm, PFTBTT = 50–200 nm. Details about the device preparation and analysis, including calculation of the mobility, were published earlier [44]

disorder in the copolymer backbone. Upon a short delay, the highest mobility is measured for the two alternating copolymers, followed by the partially alternating copolymers. The statistical copolymer has by far the lowest mobility. This could be a result of the lower TBTT content, which effectively reduces the number of low-energy transport sites. In addition, the high structural disorder is likely to introduce an increased energetic disorder and could result in the formation of electron traps, as described ahead.

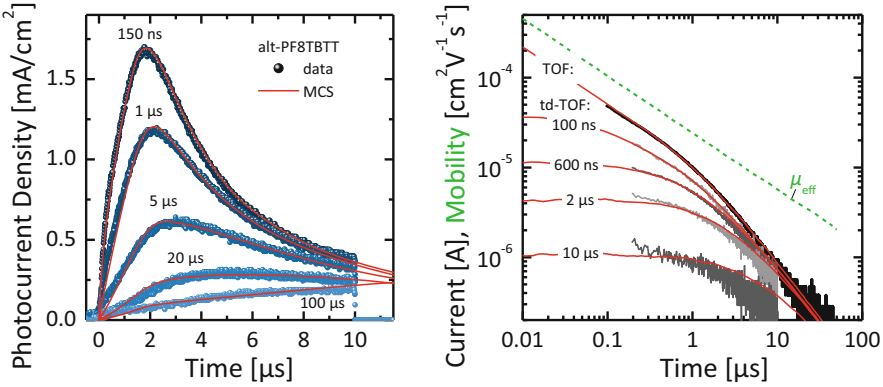

Fig. 9 (*left*) Photogenerated charge extraction by linearly increasing voltage (photo-CELIV) transients for alt-PF8TBTT measured in a charge-generation layer device. All transients are shifted along the time axis to set the beginning of the extraction pulse to $t = 0$. The delay between photoexcitation and the beginning of the linearly increasing extraction voltage is indicated on each transient. (*right*) Time-of-flight (TOF) and time-delayed-TOF transients, where the delay time is indicated for the latter. In both graphs, *red lines* display results from Monte Carlo simulations assuming a trapping and release–dominated electron transport. The effective mobility (μ_{eff}) in such a system is time dependent and undergoes a power law decay as it is displayed (*green dashed line*)

In addition to the large differences in the magnitude of the mobilities, we observe that the charge carrier mobility for several copolymers is not constant in time but instead displays a severe relaxation. Although described before, time-dependent mobilities are still a poorly understood phenomenon and were thus further investigated. The fastest mobility decay is observed for alt-PF8TBTT, where it follows a power law decay. This is accompanied by a change in the shape of the photo-CELIV current transients (Fig. 9), which shows a decreasing and shifting photocurrent signal that lacks a clear maximum after prolonged delay. The charge-generation-layer technique also allowed us to perform time-of-flight (TOF) and a newly developed technique called time-delayed TOF (td-TOF) measurements on the same devices. Introducing a delayed extraction renders the characteristic kink in the TOF transient to disappear.

The anomalous shape of the photocurrent transients and how it is related to the mobility relaxation was further analyzed with Monte Carlo–type computer simulations. A time-dependent mobility has been observed in systems where the charge transport is affected by an exponential density of trap states [45]. Within this so-called multiple trapping model, trapped charges must be thermally activated to a manifold of transport states. To account for the high electrical fields that are applied at the end of a photo-CELIV pulse, an additional field-dependent detrapping mechanism has been introduced [44]. With this model, all transient photocurrent experiments conducted on alt-PF8TBTT could be simulated with a single parameter set as can be seen in Fig. 9. Thus, we may conclude that the observed changes in

the characteristics of the transients are related to the continuous relaxation of the electron mobility caused by the presence of an exponential distribution of electron traps.

Trap-dominated electron currents are a common phenomenon in steady-state current voltage measurements of conjugated polymers. It has been assumed previously that this might be the result of chemical defects that are unintentionally introduced during the synthesis and processing of organic semiconductors [46]. In contrast to this theory, we observe strong differences in the transport characteristics of alt-PF8TBTT and PF8/12TBTT, in a way that one is trap-controlled while the other is trap-free. However, both have been synthesized by following the same procedures and both copolymers are different only in the length of the solubilizing side chains. Also, the device preparation and characterization were carried out under the same conditions. We therefore propose that trapping in alt-PF8TBTT is caused by effects related to the molecular structure or microscopic morphology rather than originating from chemical defects [44]. Conformational disorder in amorphous poly(fluorene) aggregates has been found to increase upon octyl-substitution by combined molecular dynamics and density functional theory–based simulations [47]. This increased energetic disorder might also be the origin of the mobility relaxation of the statistical copolymer stat-PF2/6TBTT. This raises the question of the missing trapping effects in partially alternating copolymers that were shown before to comprise a significantly broadened energy landscape. However, transport in these copolymers might be dominated by the additionally formed aggregate states (Fig. 6), which are lower in energy [48]. The important role of aggregate states for electron transport was recently described for a high-mobility D–A copolymer [13].

The various effects observed in electron transport characteristics underline the importance of the backbone regularity of D–A -copolymers. Even small imperfections in the alternation of D–A units will have negative effects on the charge transport because of a significant increase in energetic disorder. However, the formation of aggregate or crystalline phases might compensate for the increased disorder, which increases the complexity of the interplay between energetic and transport properties. Moreover, side chains provide an important parameter for optimizing the copolymers.

5 Application in Bilayer Solar Cells

To investigate the correlation between the electronic parameters of the newly synthesized acceptor polymers and the final photovoltaic properties, we prepared bilayer solar cells using the interlayer approach. We chose this rather simple device structure to avoid the complexity that goes along with the intermixed morphology in bulk heterojunction polymer blends. We formed bilayer all-polymer solar cells by first preparing a thin insoluble donor layer consisting of poly(3-hexylthiophene) on which a thicker layer of the PFTBTT copolymers is spin coated [44]. The investigation starts again with a detailed analysis of the interlayer, followed by

the description of the energy-level alignment at the P3HT/PFTBTT heterojunction. Finally, we studied the effect of depositing a metal top contact to determine the energetic structure of the complete device. This section presents the photovoltaic properties and interprets them in view of the measured optical, energetic and charge transport properties.

5.1 PFTBTT Copolymers as Acceptors Combined with P3HT

5.1.1 Energy-Level Alignment at the P3HT/PFTBTT Interface

The P3HT-interlayer (P3HT-IL) is an insolubilized P3HT film with a layer thickness of 3–6 nm [49]. As can be seen in Fig. 10, Φ and the position of the VB onset of the P3HT-IL are identical compared to a spin-coated P3HT film with a thickness of 10 nm. Unfortunately, this only holds for the same material and solvent. Different energy-level positions are observed for P3HT with different molecular weights, regioregularities, solvents, or preparation conditions or that come from different providers [50, 51]. All these parameters influence the order of the individual

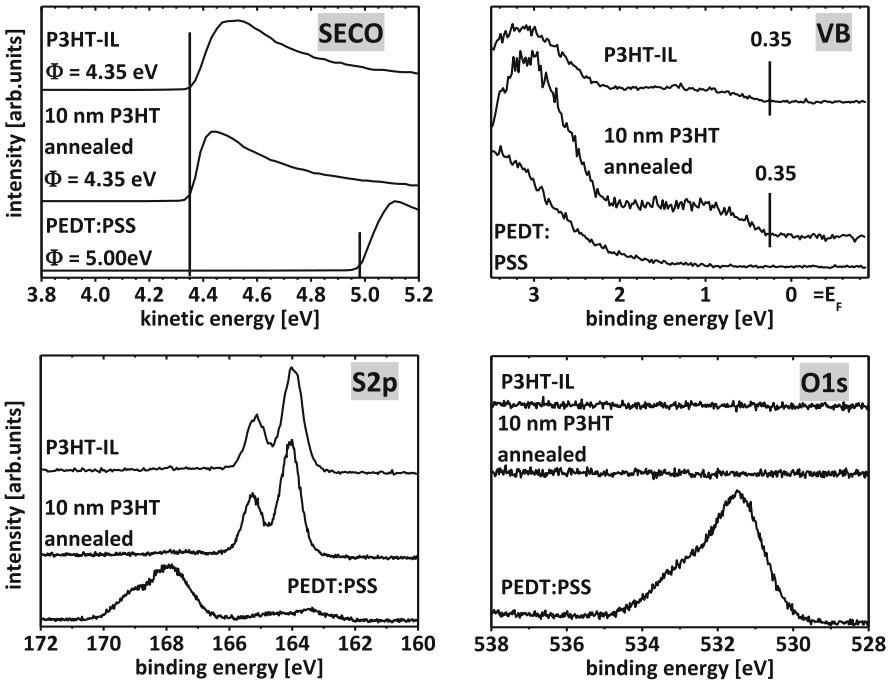

Fig. 10 Secondary electron cutoff, valence band, S2p, and O1s core-level spectra of the pristine PEDT:PSS substrate, a 10-nm P3HT film annealed in ultrahigh vacuum, and those of the P3HT-IL

polymer chains within the film and the micrometer morphology of the polymer layer. In particular, the tilt angle of the polymer backbone plane with respect to the substrate influences the IE of the films [52, 53]. Here, as shown in Fig. 10, Φ of the pristine PEDT:PSS layer below was decreased by 0.65 eV because of the formation of the P3HT-IL. The formed interface dipole at the anode–donor interface defines the effective Φ of this material combination [54]. It is thus important when correlating material parameters and device performance to note that the effective Φ is the relevant value for the anode side in the device in contrast to Φ of the bare PEDT:PSS anode. Additionally, no holes or pinholes can be observed in the P3HT-IL. This is indicated by the complete attenuation of all substrate core-level features due to the interlayer formation (see core-level region spectra in Fig. 10). Therefore, the P3HT-IL can be used to study the energy-level alignment at the intimate P3HT-IL/PF8TBTT and P3HT-IL/PF8/12TBTT interface, preventing direct contact between the acceptor polymer and the anode material as well as intermixing of the two polymers.

The VB spectra of the alternating and partially alternating PF8TBTT and PF8/12TBTT spin coated on the P3HT-IL (Fig. 11) show no more intensity close to E_F originating from the underlying P3HT-IL. The absence of P3HT features is evidence for complete coverage of the P3HT-IL by the PFTBTT copolymers and the absence of pronounced polymer intermixing. The film thickness of all polymers was ∼20 nm. The sample Φ (see SECO in Fig. 11) increased after film formation for all copolymers up to 4.80 eV. Adding the measured Φ values to the determined VB onset, we found that the resulting IEs range from 5.40 and 5.45 eV for part- and alt-PF8TBTT to 5.50 eV and 5.60 eV for part- and alt-PF8/12TBTT, respectively. It is important to note that all calculated IEs are much higher compared to the effective Φ of the PEDT:PSS/P3HT-IL substrate. Therefore, the Φ increase caused by the deposition of copolymers was unexpected. In contrast to the measured Φ shifts at the P3HT-IL/copolymer interface, vacuum-level alignment was predicted for this material combination [55, 56]. However, as noted before (see Sect. 3.1),

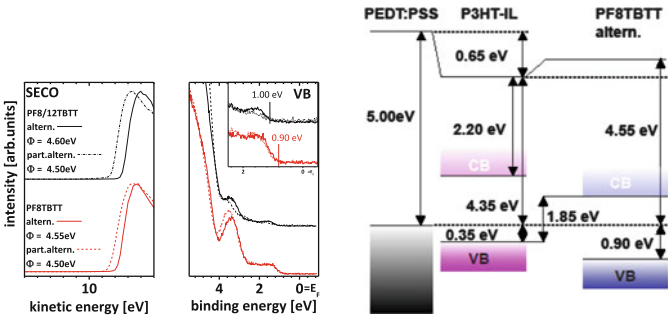

Fig. 11 (*left*) Secondary electron cutoff and valence band (VB) of the alternating and partially alternating PF8TBTT (*red*) and PF8/12TBTT (*black*) spin coated from chloroform solution on P3HT-IL. (*right*) Energy-level scheme at the P3HT-IL/alt-PF8TBTT interface. Work function (Φ), VB onset, and photovoltaic gap (Δ_{PVG}) for all copolymers investigated are summarized in Table 2

the low density of gap states in PF8TBTT and PF8/12TBTT does not show up in photoemission (because of their low density) but can cause pinning of E_F far in the gap [37].

UPS results for the PEDT:PSS/P3HT-IL/alt-PF8TBTT interfaces are summarized in the energy-level diagram in Fig. 11. The position of the P3HT conduction band (CB) onset was calculated by subtracting the transport gap of 2.5 eV from the VB onset position [57]. The transport gap of alt-PF8TBTT was estimated to be 2.4 eV (optical gap of 1.9 eV plus exciton binding energy of 0.5 eV). It is well accepted in the literature that the upper limit for the V_{OC} is given by the photovoltaic gap (Δ_{PVG}; the difference between the VB onset of the donor and the CB onset of the acceptor) in organic heterojunction solar cells [58, 59]. In the present case of P3HT and alt-PF8TBTT, a photovoltaic gap of 1.85 eV was determined from the energy-level diagram in Fig. 11. This value is, however, significantly larger than the energy difference between the ionization energy of P3HT (4.70 eV) and the electron affinity of the alt-PF8TBTT (3.05 eV) assuming vacuum-level alignment, which would yield 1.65 eV. This indicates the importance of directly determining the interfacial D–A energy-level alignment. However, compared to the measured V_{OC} of 1.21 eV in the device (see Table 3), the UPS-derived value of the photovoltaic gap was 0.64 eV larger. Losses on the order of 0.5 eV and above, as deduced directly from the UPS experiments, are in agreement with previously determined energetic losses in bulk heterojunction solar cells of alt-PF8TBTT and PCBM and equal those found in some of the best photovoltaic D–A combinations, which show a typical loss of 0.5–0.7 eV measured from the energy of the charge-transfer state [60, 61]. The energy difference between V_{OC} and the photovoltaic gap is evidence for nonradiative recombination processes and energetic disorder.

5.1.2 Full Electronic Structure

In order to acquire the energetic structure of a complete solar cell device, we used UPS to analyze the deposition of the samarium (Sm) top electrode. Figure 12 shows SECO and VB spectra for different Sm thicknesses. The sample Φ drastically decreased to 2.3 eV because of the deposition of 10 Å Sm and stabilized at 2.60 eV for a higher Sm coverage. The intensity of all copolymer-related VB features decreased from the early stage of interface formation. For increasing Sm coverage, the alt-PF8TBTT features shifted to a higher binding energy (BE) (Fig. 12) and the emission intensity from Sm close to the Fermi level increased. The PFTBTT features are not broadened but are clearly visible up to a Sm coverage of 2 Å. The energy-level shift of the alt-PF8TBTT features to a higher BE represents the magnitude of the built-in field because of Fermi-level alignment between the two electrodes in the device. As Fig. 12 shows, the maximum of the localized peak (at ∼3.5 eV BE) was clearly shifted to a higher BE by ∼0.85 eV. Unfortunately, the final position of the VB onset cannot be determined because of the rapid attenuation of the features above 2 Å Sm coverage. Because the EA of the alt-PF8TBTT of 3.35 eV (see previous section) is much larger than the Sm Φ, we expect an interfacial dipole

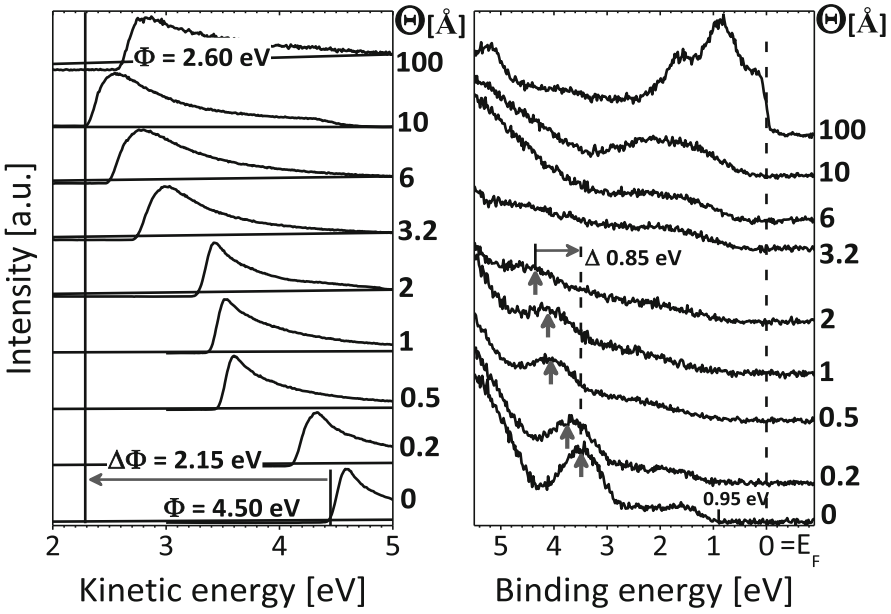

Fig. 12 Secondary electron cutoff (*left*) and photoemission spectra of the valence region (*right*) and for increasing Sm coverage (Φ) on a P3HT-IL/alt-PF8TBTT heterojunction. *Black arrows* indicate the position of the lowest localized π band of the alt-PF8TBTT

(ID) to be formed at the polymer/Sm interface as a result of unoccupied states of the polymer being pinned at E_F of the Sm electrode.

To determine the strength of the ID at the alt-PF8TBTT/Sm interface, we performed the reverse experiment—spin coating an alt-PF8TBTT film onto a pristine Sm layer (see Fig. 13). We first investigated the influence of the deposition method on the pristine Sm film by spin coating the pure solvent on a freshly evaporated Sm film. After the spin coating, the C and O concentrations on the Sm surface drastically increased [see X-ray photoelectron spectroscopy (XPS) survey spectra in Fig. 13]. In parallel, Φ of the Sm surface decreased by 0.2 eV and the VB region spectrum (see Fig. 13) became similar to that of SmO_X [62], as clearly indicated by the vanished photoelectron intensity at E_F. Both UPS and XPS clearly showed a complete oxidation of the Sm surface and the copolymer was deposited on a thin SmO_X film rather than on pristine Sm. Nevertheless, investigations of the energy-level alignment at the SmO_X/alt-PF8TBTT interface include important information about the pinning position of the Sm Fermi level with respect to the occupied states of the alt-PF8TBTT, where the E_F pinning was again induced by unoccupied states of the copolymer. These become occupied by electrons close to the interface and cause the formation of an interface dipole and consequently the observed Φ increase to 3.40 eV. The levels to which electrons are transferred could be either the CB minimum or states below if tail states in the gap close to

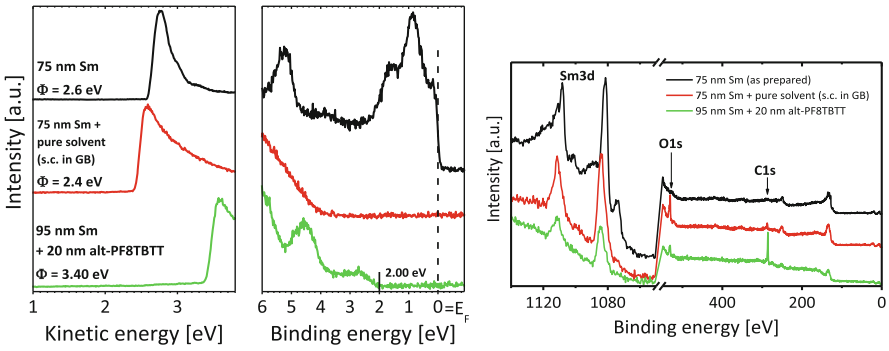

Fig. 13 Ultraviolet photoelectron spectroscopy spectra of the secondary electron cutoff (*left*) and valence region (*center*) as well as X-ray photoelectron spectroscopy (XPS) survey spectra (*right*) of a 75-nm Sm film vapor deposited in ultrahigh vacuum (UHV) before (*black*) and after direct transfer to an N_2-filled glove box (GB) in low-vacuum conditions (10^{-2} mbar) (*red line*). The *green* spectrum represents the XPS survey spectrum of a 20-nm alt-PF8TBTT film spin coated in an N_2-filled GB on a pristine 95-nm Sm film vapor deposited in UHV

the CB exist. The energy value at which the CB minimum becomes pinned above E_F depends on the effective density of states, the distribution of tail states, and the number of charges that needed to be transferred to reach an electronic equilibrium. However, the resulting interface dipole at the SmO_X/alt-PF8TBTT interface was determined to 1.00 eV. As shown in Fig. 13, the VB onset of the copolymer is located 2.00 eV below E_F. This is 0.25 eV higher than the last measurable position of the alt-PF8TBTT VB onset (at 1.75 eV BE) in the reverse deposition sequence described earlier.

In conclusion, Fermi-level alignment between the ITO/PEDT:PSS substrate and the Sm film is established independently of the polymer heterojunction in between. This is clearly indicated by the position of the Sm E_F at 0 eV BE. Note that Fermi-level alignment across the heterojunction is comparable to short-circuit conditions in a device. By combining the results of the photoemission experiments, one can derive the full electronic structure across all interfaces in the P3HT-IL/alt-PF8TBTT solar cell, as shown in Fig. 14 [63]. The established built-in field across the heterojunction at closed-circuit conditions can be determined to 1.10 eV. As can be seen in the energy-level diagram, because of the built-in field, the energy levels of the alt-PF8TBTT are tilted and Fermi-level alignment is established across the layers.

5.1.3 Bilayer Solar Cells with PFTBTT Copolymers as Acceptors

Investigating the effects of altered energetic disorder and charge transport properties on the photovoltaic performance of the different PFTBTT copolymers was a central aim of this study.

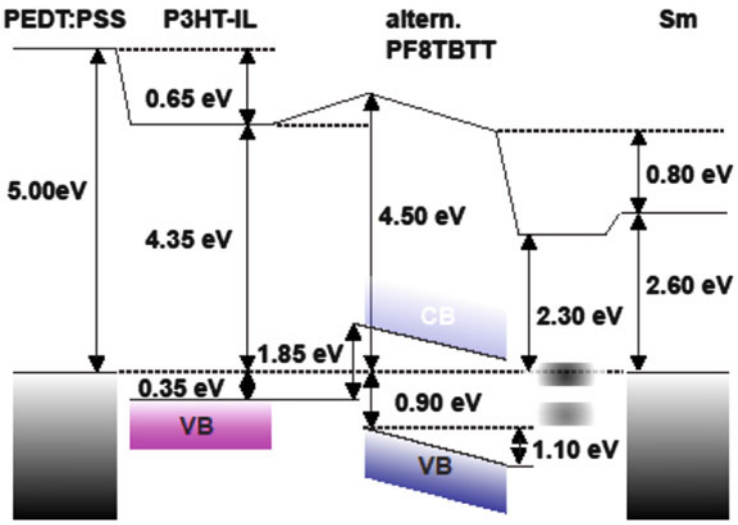

Fig. 14 Schematic energy-level diagram of a P3HT-IL/alt-PF8TBTT bilayer solar cell

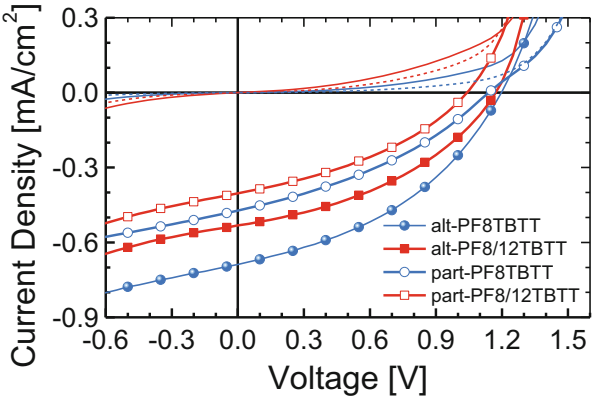

Fig. 15 Current–voltage characteristics of bilayer solar cells comprising PFTBTT copolymers as acceptor on top of a P3HT-IL measured at 100 mA/cm^2 (*symbols*) and in the dark (*lines*, *solid* = alt, *dashed* = part). Devices were annealed for 10 min at 140 °C. Device structure: ITO/PEDT:PSS/P3HT-interlayer(∼3 nm)/PFTBTT(40 nm)/Ca(20 nm)/Al(100 nm)

Typical current–voltage characteristics and solar cell parameters of P3HT-IL–based bilayer solar cells comprising different PFTBTT copolymers as acceptor are displayed in Fig. 15 and Table 3, respectively. From all copolymers, solar cells with statistical PFTBTT copolymer exhibit very low short-circuit currents, about an order of magnitude smaller than the current measured for alternating copolymers. Additionally, the solar cells suffer from very low fill factors of about 20 % and small open-circuit voltages. Hereby, we found that neither the structure of the

side chains or that of the backbone (via varying TBTT fractions) considerably affects the solar cell performance of statistical copolymers. Since the statistical copolymer had the lowest electron mobility measured, the mobility imbalance between donor (P3HT) and acceptor (PFTBTTs) polymer was the largest [14]. However, the low photocurrent, fill factor, and open-circuit voltage—together all a clear sign for recombination-limited solar cells—clearly show that an increased mobility imbalance does not improve the photovoltaic performance. In fact, the severe recombination losses of free charge carriers are likely to be introduced by the accumulation of charges in the device, a direct consequence of the low electron mobility determined for stat-PF2/6TBTT (Fig. 8) [64]. Thus, we conclude that the potentially positive effect of a mobility imbalance is removed by an increased recombination. This concept might indeed only work if a high-mobility donor and acceptor component are combined to ensure an efficient separation of the electron and hole densities inside the active layer.

Compared to the statistical copolymers, partially alternating PFTBTTs show a much better photovoltaic response, but they are clearly not as good as the alternating derivatives. This is true for both side chain variants. Overall, the photocurrent follows almost the same trend as the electron mobility shown in Fig. 8. Only alt-PF8TBTT seems to fall away from this trend; however, as a result of the mobility relaxation, alt-PF8TBTT can be expected to have the highest mobility on timescales below a picosecond, which are more relevant for charge carrier generation [23, 24, 65]. Consequently, our results give some evidence that the charge separation efficiency benefits from a high electron mobility. On the other hand, our results show that the larger degree of disorder observed for the two partially alternating copolymers (Fig. 6) does not improve the photovoltaic performance as predicted by theory for ideal bilayer structures.

In addition to the impact of the mobility and disorder, we analyzed the interplay between the energetic structure and the photovoltaic parameters. We expected the open-circuit voltage to have a direct correlation to the experimentally determined energetic structure. In particular, we were investigating if the reduced optical bandgap of the partially alternating copolymers and the experimentally determined photovoltaic gap (Table 2) could be directly correlated to the open-circuit voltage. Indeed, the open-circuit voltage and the photovoltaic gap decreased in parallel when we compared alternating with partially alternating polymers, as can be seen in Table 3, although the correlation of the open-circuit voltage as a function of

Table 2 Work function F, valance band (VB) onset, and photovoltaic gap (Δ_{PVG}) for the different copolymer films deposited on P3HT-IL

Copolymer	Φ (eV)	VB onset (eV)	Δ_{PVG} (eV)
alt-PF8TBTT	4.55	0.90	1.85
part-PF8TBTT	4.50	0.90	1.65
alt-PF8/12TBTT	4.60	1.00	1.75
part-PF8/12TBTT	4.50	1.00	1.55

Table 3 Solar cell performance of alternating (alt), partially alternating (part), and statistical (stat) PFTBTT copolymers. All devices were annealed at 140 °C for 10 min before evaporation of the top contact. The structure of the solar cells was ITO/PEDT:PSS/P3HT-interlayer(∼3 nm)/PFTBTT(40 nm)/Ca(20 nm)/Al(100 nm)

PFTBTT	V_{OC} (V)	J_{SC} (mA/cm^2)	FF (%)	η_{PCE} (%)	$\Delta_{PVG}-V_{OC}$ (eV)
alt-PF8TBTT	1.21	0.690	40	0.33	0.64
alt-PF8/12TBTT	1.17	0.530	40	0.24	0.58
part-PF8TBTT	1.15	0.470	35	0.19	0.50
part-PF8/12TBTT	1.04	0.400	30	0.15	0.51
stat-PF2/6TBTT (30 % TBTT)	0.89	0.056	20	0.01	–

FF fill factor, *PCE* power conversion efficiency
Values for Δ_{PVG} were taken from Table 2

the photovoltaic gap was not linear. Because of different recombination kinetics at the different polymer heterojunctions and the relatively high dark currents observed in the interlayer devices, this nonlinear correlation was unexpected. A direct comparison of Δ_{PVG} and V_{OC} for alt-PF8TBTT and part-PF8TBTT revealed that the loss term (Δ_{PVG} – V_{OC}) was 0.14 eV larger for alt-PF8TBTT than for part-PF8TBTT. Interestingly, this difference corresponds well with the reduction in the optical gap for the partially alternating copolymer. Consequently, the loss mechanism in the device seemed to be similar for alt-PF8TBTT and part-PF8TBTT, and the V_{OC} was directly limited by the energy-level alignment at the heterojunction, as we determined with UPS. We observed the same trend for the two PF8/12TBTT copolymers although the comparison was obscured by the higher dark currents, which resulted in a smaller difference of only 0.07 eV between the loss terms. Thus, we were able to link the experimentally determined energetic structure of several all-polymer heterojunctions to their photovoltaic performance, providing a new and more precise way to analyze the interplay between energy-level alignment and solar cell performance.

6 Summary

Our results show that a larger degree of disorder and mobility imbalance—as we introduced to the photovoltaic systems through chemical modifications of the acceptor polymers—does not improve the photovoltaic performance. The main reason for this lack of improvement is a decrease in the charge carrier mobility for polymers that do not comprise a strictly alternating copolymer structure. Ultimately, this inefficient electron transport increases the bimolecular recombination of free charges and drastically reduces device performance. This finding is in accordance with recent computer simulations and analytical results that predict the charge carrier mobilities of organic solar cells will have a tremendous influence on the *J*–*V* characteristics [14, 64]. Moreover, we observed that mainly the photocurrent

benefits from a high electron mobility, which could be related to improved charge carrier dissociation at the heterojunction. Finally, we were able to correlate the energetic structure measured with UPS to the open-circuit voltage of the complete solar cell devices. Overall, our results will help guide researchers toward making further improvements to this successful class of synthetic semiconducting copolymers.

Acknowledgment The authors thank the DFG for funding within the DFG Priority Program 1355 "Elementary Processes of Organic Photovoltaics." This report is based on results obtained by the collaboration of project no. 15 ("Tuning the Optical and Charge-Transporting Properties of the Electron-Accepting Phase in Polymer Solar Cells") and project number 11 ("Electronic Properties of Interfaces with Conjugated Polymers and Polyelectrolytes").

References

1. Zhang Z-G, Wang J (2012) J Mater Chem 22:4178
2. Kang I, Yun H-J, Chung DS, Kwon S-K, Kim Y-H (2013) J Am Chem Soc 135:14896
3. Tseng H-R, Phan H, Luo C, Wang M, Perez LA, Patel SN, Ying L, Kramer EJ, Nguyen T-Q, Bazan GC, Heeger AJ (2014) Adv Mater 26:2993
4. Yi Z, Wang S, Liu Y (2015) Adv Mater 27:3589
5. Guo X, Facchetti A, Marks TJ (2014) Chem Rev 114:8943
6. Lin Y, Zhan X (2014) Mater Horiz 1:470
7. Steyrleuthner R, Schubert M, Jaiser F, Blakesley JC, Chen Z, Facchetti A, Neher D (2010) Adv Mater 22:2799
8. Yan H, Chen Z, Zheng Y, Newman C, Quinn JR, Dotz F, Kastler M, Facchetti A (2009) Nature 457:679
9. Kang H, Uddin MA, Lee C, Kim K-H, Nguyen TL, Lee W, Li Y, Wang C, Woo HY, Kim BJ (2015) J Am Chem Soc 137:2359
10. Mori D, Benten H, Okada I, Ohkita H, Ito S (2014) Energy Environ Sci 7:2939
11. Ye L, Jiao X, Zhou M, Zhang S, Yao H, Zhao W, Xia A, Ade H, Hou J (2015) Adv Mater. doi:10.1002/adma.201503218
12. Li W, Roelofs WSC, Turbiez M, Wienk MM, Janssen RAJ (2014) Adv Mater 26:3304
13. Steyrleuthner R, Di Pietro R, Collins BA, Polzer F, Himmelberger S, Schubert M, Chen Z, Zhang S, Salleo A, Ade H, Facchetti A, Neher D (2014) J Am Chem Soc 136:4245
14. Marsh RA, Groves C, Greenham NC (2007) J Appl Phys 101:083509
15. Offermans T, Meskers SCJ, Janssen RAJ (2005) Chem Phys 308:125
16. Yang F, Forrest SR (2008) ACS Nano 2:1022
17. Svensson M, Zhang F, Veenstra SC, Verhees WJH, Hummelen JC, Kroon JM, Inganäs O, Andersson MR (2003) Adv Mater 15:988
18. Groves C, Marsh RA, Greenham NC (2008) J Chem Phys 129:114903
19. Huang Y, Westenhoff S, Avilov I, Sreearunothai P, Hodgkiss JM, Deleener C, Friend RH, Beljonne D (2008) Nat Mater 7:483
20. Liu J, Choi H, Kim JY, Bailey C, Durstock M, Dai L (2012) Adv Mater 24:538
21. McNeill CR, Abrusci A, Zaumseil J, Wilson R, McKiernan MJ, Burroughes JH, Halls JJM, Greenham NC, Friend RH (2007) Appl Phys Lett 90:193506
22. McNeill CR, Halls JJM, Wilson R, Whiting GL, Berkebile S, Ramsey MG, Friend RH, Greenham NC (2008) Adv Funct Mater 18:2309
23. McNeill CR, Westenhoff S, Groves C, Friend RH, Greenham NC (2007) J Phys Chem C 111:19153
24. Mori D, Benten H, Ohkita H, Ito S (2015) Adv Energy Mater 5:1500304

25. Mori D, Benten H, Ohkita H, Ito S, Miyake K (2012) ACS Appl Mater Interfaces 4:3325
26. Yan H, Collins BA, Gann E, Wang C, Ade H, McNeill CR (2012) ACS Nano 6:677
27. Kodomari M, Satoh H, Yoshitomi S (1988) J Org Chem 53:2093
28. Baillargeon VP, Stille JK (1986) J Am Chem Soc 108:452
29. Li J-H, Liang Y, Wang D-P, Liu W-J, Xie Y-X, Yin D-L (2005) J Org Chem 70:2832
30. Ellinger S, Ziener U, Thewalt U, Landfester K, Möller M (2007) Chem Mater 19:1070
31. Letizia JA, Salata MR, Tribout CM, Facchetti A, Ratner MA, Marks TJ (2008) J Am Chem Soc 130:9679
32. Mulherin RC, Jung S, Huettner S, Johnson K, Kohn P, Sommer M, Allard S, Scherf U, Greenham NC (2011) Nano Lett 11:4846
33. Nothofer H-G (2005) Dissertation, Universität Potsdam
34. Yamamoto T (1992) Prog Polym Sci 17:1153
35. Hwang J, Kim E-G, Liu J, Brédas J-L, Duggal A, Kahn A (2007) J Phys Chem C 111:1378
36. Koch N, Elschner A, Rabe JP, Johnson RL (2005) Adv Mater 17:330
37. Lange I, Blakesley JC, Frisch J, Vollmer A, Koch N, Neher D (2011) Phys Rev Lett 106:216402
38. Sueyoshi T, Fukagawa H, Ono M, Kera S, Ueno N (2009) Appl Phys Lett 95:183303
39. Garreau S, Leclerc M, Errien N, Louarn G (2003) Macromolecules 36:692
40. Steyrleuthner R, Schubert M, Howard I, Klaumünzer B, Schilling K, Chen Z, Saalfrank P, Laquai F, Facchetti A, Neher D (2012) J Am Chem Soc 134:18303
41. Schubert M, Dolfen D, Frisch J, Roland S, Steyrleuthner R, Stiller B, Chen Z, Scherf U, Koch N, Facchetti A, Neher D (2012) Adv Energy Mater 2:369
42. Chua L-L, Zaumseil J, Chang J-F, Ou EC-W, Ho PK-H, Sirringhaus H, Friend RH (2005) Nature 434:194
43. Bange S, Schubert M, Neher D (2010) Phys Rev B 81:035209
44. Schubert M, Preis E, Blakesley JC, Pingel P, Scherf U, Neher D (2013) Phys Rev B 87:024203
45. Orenstein J, Kastner M (1981) Phys Rev Lett 46:1421
46. Nicolai HT, Kuik M, Wetzelaer GAH, de Boer B, Campbell C, Risko C, Brédas JL, Blom PWM (2012) Nat Mater 11:882
47. Kilina S, Dandu N, Batista ER, Saxena A, Martin RL, Smith DL, Tretiak S (2013) J Phys Chem Lett 4:1453
48. Noriega R, Rivnay J, Vandewal K, Koch FPV, Stingelin N, Smith P, Toney MF, Salleo A (2013) Nat Mater 12:1038
49. Huang DM, Mauger SA, Friedrich S, George SJ, Dumitriu-LaGrange D, Yoon S, Moulé AJ (2011) Adv Funct Mater 21:1657
50. Chang J-F, Sun B, Breiby DW, Nielsen MM, Sölling TI, Giles M, McCulloch I, Sirringhaus H (2004) Chem Mater 16:4772
51. Zen A, Pflaum J, Hirschmann S, Zhuang W, Jaiser F, Asawapirom U, Rabe JP, Scherf U, Neher D (2004) Adv Funct Mater 14:757
52. Hao XT, Hosokai T, Mitsuo N, Kera S, Okudaira KK, Mase K, Ueno N (2007) J Phys Chem B 111:10365
53. Heimel G, Salzmann I, Duhm S, Rabe JP, Koch N (2009) Adv Funct Mater 19:3874
54. Frisch J, Vollmer A, Rabe JP, Koch N (2011) Org Electron 12:916
55. Braun S, Salaneck WR, Fahlman M (2009) Adv Mater 21:1450
56. Hwang J, Wan A, Kahn A (2009) Mater Sci Eng R Rep 64:1
57. Kanai K, Miyazaki T, Suzuki H, Inaba M, Ouchi Y, Seki K (2010) Phys Chem Chem Phys 12:273
58. Dennler G, Scharber MC, Brabec CJ (2009) Adv Mater 21:1323
59. Rand BP, Burk DP, Forrest SR (2007) Phys Rev B 75:115327
60. Burke TM, Sweetnam S, Vandewal K, McGehee MD (2015) Adv Energy Mater 5:1500123
61. Vandewal K, Tvingstedt K, Gadisa A, Inganäs O, Manca JV (2010) Phys Rev B 81:125204
62. Kuriyama T, Kunimori K, Kuriyama T, Nozoye H (1998) Chem Commun 501. doi:10.1039/A707932J

63. Frisch J, Schubert M, Preis E, Rabe JP, Neher D, Scherf U, Koch N (2012) J Mater Chem 22:4418
64. Würfel U, Neher D, Spies A, Albrecht S (2015) Nat Commun 6:6951
65. Schubert M, Collins BA, Mangold H, Howard IA, Schindler W, Vandewal K, Roland S, Behrends J, Kraffert F, Steyrleuthner R, Chen Z, Fostiropoulos K, Bittl R, Salleo A, Facchetti A, Laquai F, Ade HW, Neher D (2014) Adv Funct Mater 24:4068